Flux Based Control of AMBs Using Integrated Ultra-Thin Flexible Bismuth Hall Sensors

Falk Bahr[1,*], Michael Melzer[2], Daniil Karnaushenko[2,3], Denys Makarov[2],
Dmitriy Karnaushenko[2], Jens Ingolf Mönch[2], Dominic Malane[1],
Oliver G. Schmidt[2,3] and Wilfried Hofmann[1]

[1]Elektrotechnisches Institut, Technische Universität Dresden, Germany
[2]Institute for Integrative Nanosciences, IFW Dresden, Germany
[3]Material Systems for Nanoelectronics, Chemnitz University of Technology, Germany

Abstract

To increase stiffness and precise rotor positioning of active magnetic bearings (AMB), flux based control algorithms were suggested. However, the typical thickness of air gaps in AMBs is too small to apply conventional magnetic field sensors with a typical thickness of more than 500 µm. Furthermore, the curved surfaces of the stator poles require a mechanically flexible sensor design. Here, we propose a flexible Bismuth based Hall sensor with a total thickness of only 80 µm including encapsulation. After wiring the sensors have a maximum height of 280 µm and could be mounted onto curved surfaces. The fabricated sensors were characterized and the influence of size, temperature and bending radius on the Hall sensitivity was determined. On a proof-of-concept level we demonstrated the performance of the flexible magnetic field sensors to control an one-axis AMB with a levitating ball. Several algorithms using flux density measurements were tested and compared to conventional control strategies.

1 Introduction

Precise positioning of the rotor in AMBs is limited by the frequency dependent low stiffness. We focus on the increase of dynamic stiffness and precision using flux based control algorithms. In this respect, integration of a magnetic field sensor in a small air gap (< 500 µm) is the main challenge regarding the sensor´s design, manufacturing and assembly. For this purpose, ultra-thin and flexible sensors detecting out-of-plane magnetic fields up to 2.2 T with high precision and reliability need to be developed. Within the last 20 years the potential of flux based control for AMB has been shown, especially for high precision applications [1,2]. On the other hand ideas of sensorless (position) controls with flux density measurement [3] or flux observer [4] were presented. Nowadays, both aspects are important concerning increasing requirements in machining on one hand as well as cost savings for standard AMBs on the other hand. Thus, development of magnetic field sensors in combination with flux based control strategies is a top issue regarding AMB systems as well as for bearingless drives.

In recent years various technologies to achieve flexible electronics have been suggested and some were already brought to the stage of market-ready commercial products [5,6]. Inorganic semiconductor and metal based electronic components can be fabricated onto compliant polymeric substrates by means of thin film technology. Even flexible [7-9] and stretchable [10,11] magnetoelectronic elements have recently been realized. However, these magnetoresistive elements are typically applied only for in-plane magnetic field measurements and reveal a maximum sensitivity in a low field regime of several mT, which is not suitable for AMB applications.

For the required field range of about 2 T Hall effect based sensors are the favorable choice, as they provide a linear voltage response up to high magnetic fields. Recently, arrangements of semiconductor based Hall sensors have been fabricated on a polyimide substrate using SOI-wafers [12]. However, the flexibility of the substrate was used to rearrange the planar probes into a 3D structure by folding, rather than bending the sensors themselves. In order to fabricate intrinsically flexible Hall probes, in this work we realized thin Bismuth (Bi) films on plastic foil structured into a cross geometry. After characterization of the prepared sensors, we optimized their sensitivity by varying parameters like cross size, operation temperature and bending radius.

The functionality was tested in an experimental levitating ball setup resembling a monopole AMB. Here, we were able to implement several flux based control algorithms, where the measured air gap flux density is used as

*Contact: E-Mail: falk.bahr@tu-dresden.de; Helmholtzstraße 9, 01069 Dresden; Phone: +49 351 46335052

feedback for certain controller types. In this first experimental study with ultra-thin sensors we focused on two different control approaches with position measurement: a linear as well as a nonlinear control structure was designed and we compared linear flux density and current based control. As a final step, a flatness based control approach to improve performance is introduced as well.

2 Flux Based Control and Experimental Setup

2.1 Characteristics and Application Area

Due to contact-free operation with adjustable rotor-positioning, AMBs achieve increasing acceptance in high-speed applications, especially in manufacturing components with highly precise surfaces and special curved geometries [13]. During the last two decades, AMB-spindle systems for turning, milling and grinding have significantly improved the quality of work pieces. In case of increased precision and improved dynamic performance, certain production steps like grinding can be avoided for certain processes.

The dynamic stiffness and damping governs the AMBs behavior. Especially in case of varying loads and disturbances it is important to tune the setup to achieve a high closed loop bandwidth. To improve the dynamic parameters, flux based controls, especially algorithms supported by the measurement of air gap flux density, are favorable. Compared to conventional current based control, effects of delayed flux caused by eddy currents can be compensated by a fast inner flux density control loop. Furthermore, hysteresis does not have to be calculated during controlling. For high field setups the problem of nonlinear magnetic saturation does not appear with flux based control [14]. Moreover, with flux density measurement a temperature-sensitive permanent pre-magnetization can be detected directly.

Concerning transient response, flux based control offers reduced response times, reduced overshooting and less steady-state deviation after disturbance excitations compared to current based controls [15]. Moreover, this method is characterized by a higher robustness, smaller sensitivity with respect to noise, and offers the advantage of a collocated measurement [3,16]. Especially the latter is important to avoid positive feedback with critical self-excitation of flexible rotor structures [17].

However, for measurement of magnetic flux densities inside air gaps extra sensors have to be integrated onto the pole surfaces and additional electronic hardware is needed. For this purpose Hall sensors can be used for the non-contact measurement of the air gap induction that characterizes the magnetic force directly.

Several publications on flux based control for AMBs are already available. Abdelfatah *et al.* compared current and flux based algorithms [15]. They achieved in simulative studies smaller response times and overshooting as well as up to 90 % reduced deviation after load disturbances and an increase of dynamic stiffness. Yi *et al.* presented a high precision positioning system with force control using a Hall sensor to detect fields up to 100 mT inside an air gap of 0.6 mm [2]. A crystal growth as well as a rotating shaft setup (air gap > 1 mm) with measurement of magnetic flux density was analyzed by Zlatnik *et al.* [3] as well as Bleuler *et al.* [16]. A sensorless realization to reduce costs for position measurement system was focused on and the rotor position was recalculated by means of coil current and air gap flux density measured by commercial Hall sensors. Imlach *et al.* proposed an indirect flux measurement integrated in the back iron [18]. In this case, sensor elements do not have to be as thin as inside the active magnetic air gap between pole and rotor. However, detecting homopolar pre-magnetization is not possible with this approach. Chen *et al.* presented a flywheel controlled by decentral cascaded structure with force-feedback using Hall- and eddy current sensors for the measurement of flux and position [1]. For speeds up to 6500 rpm experimental results show an increase of dynamic stiffness and damping together with decreased influence of disturbances compared to current based control.

Despite of all these advantages, flux based control with flux density measurement is not common for industrial applications due to the large dimension of commercial magnetic field sensors.

2.2 Setup of Levitating Ball

For the first experimental analysis of the flexible Bismuth Hall sensor we used the setup of a levitating ball (Figure 1b, Table 1) to test linear and a nonlinear flux based control approaches.

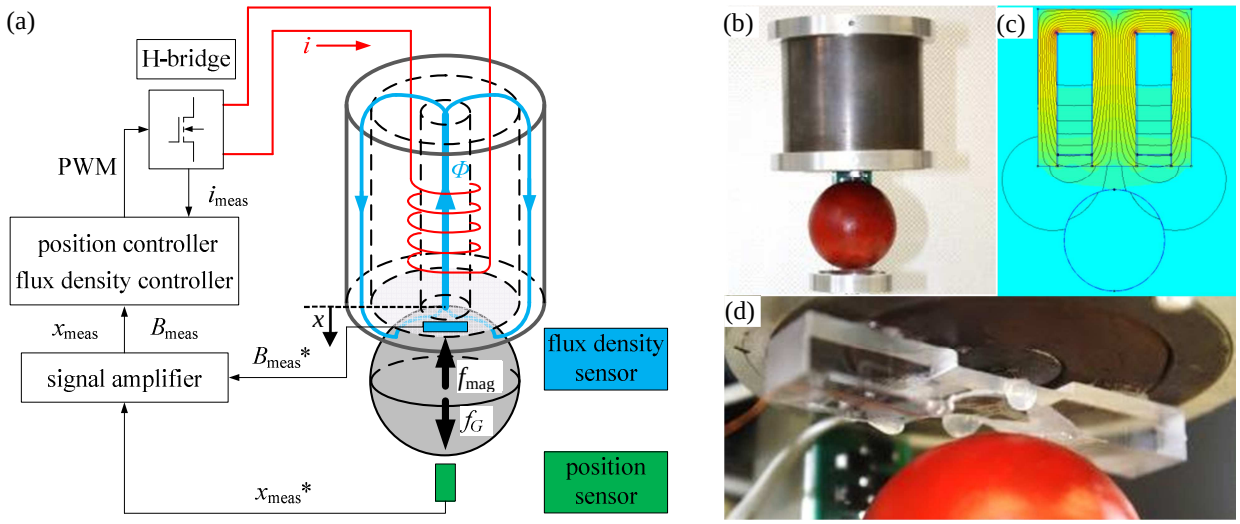

Figure 1: (a) Scheme of the test setup. (b) Levitating ball. (c) FEM of the test setup. (d) Bi Hall sensor.

In this setup, the prototype sensor is mounted inside the large air gap of up to 12 mm without risking a damage caused by mechanical collision. Figure 1a shows the basic principle of the AMB setup. The coil is implemented inside the electromagnet made of a soft magnetic composite (SMC). To achieve a ferromagnetic surface the plastic ball is coated with iron powder paint. The ball position is detected by an optical measurement system consisting of one infrared light and a photo diode array.

According to the ball geometry, the flexible Bi Hall sensor is fitted on a curved adapter (Figure 1d) being installed beneath the electromagnet core. This curved surface with a bending radius of 22 mm, resembles a typical concave shaped pole surface of AMBs. Figure 1c shows the 2D-FEM-simulation of the magnetic field (x = 10 mm, i_{max} = 6 A). Due to the inhomogeneous profile of the magnetic flux density, the sensor was mounted exactly beneath the core center to analyze characteristic curves of the AMB plant. The controller was designed based on these gained plant coefficients. As a reference for flux density measurements we integrated an additional commercial Gallium-Arsenide Hall sensor above the adapter. Due to the large air gap, maximum flux density of the setup is B_{max} = 200 mT. The complete control algorithm is implemented on a digital signal processor (DSP) based real time system including level shifting, analog-digital conversion and pulse width modulation to drive the MOSFET-H-bridge.

Parameter	Symbol	Value
Resistance coil	R	1.4 Ohm
Inductance coil	L	23 mH
Windings coil	w	100
Mass ball	m	11.2 g
Radius ball	d_{ball}	42.0 mm
Coating ball	d_{coat}	≈90 µm
Pulse frequency	f_p	10 kHz
Sampling time flux density	T_{aB}	100 µs
Sampling time coil current	T_{ai}	100 µs
Sampling time position	T_{ax}	200 µs
DC link voltage	U_{DC}	48 V

Table 1: Levitating ball setup parameters.

3 Ultra-Thin Flexible Bismuth Hall Sensor

3.1 Basics of Hall effect

The Hall effect describes the development of a voltage perpendicular to an electrical current in the presence of a magnetic field. The voltage difference arises by means of a Lorentz force acting on the charge carriers that move nonparallel to the field direction. This effect is used in Hall probes to measure magnetic flux densities that are perpendicular to a thin layer along which the electrical current is passed. In this case, the Hall voltage is measured

within the layer, perpendicular to the current, and rises linear with the magnetic field value. The sensitivity of a Hall probe (i.e. the ratio of the induced voltage difference to the measured field at a certain current) is dependent on the density, mobility and type of contributing charge carriers in the conducting layer. Therefore, mostly semiconductors are used to fabricate efficient Hall probes, because these properties can be precisely tuned my means of doping.

However, the Hall effect exists in every conductive material, and among metals Bismuth shows by far the strongest Hall effect, mainly due to the low density of its conducting electrons. The advantages of using Bismuth for Hall probes are mainly the cost effective preparation and structuring by standard thin film deposition and lithographic methods [19]. This is in particular interesting for thin and flexible sensors, as metal films can be deposited on various substrates including polymers and plastic foils [20]. Furthermore, due to its negligible surface charge depletion effects [21] Bi Hall probes show significant signal-to-noise ratio at room temperature even at sub-µm lateral sizes, which is not the case for conventional semiconducting sensors. On the other hand, the preparation of large area Hall probes (e.g. for spatial averaging of the magnetic field) remains cost efficient with deposited metal films in contrast to doped semiconductors.

3.2 Sensor Preparation

We deposited 2 µm thick Bi films on 25 µm thin, flexible and transparent sheets of Polyether ether ketone (PEEK) (Victrex® aptiv® Biax-025) by HF magnetron sputter deposition (base pressure: 5×10^{-7} mbar, Ar sputter pressure: 1×10^{-3} mbar, deposition rate: ≈5 Å/sec) at room temperature. PEEK is known among polymeric materials for its high mechanical, thermal, and chemical stability and is therefore used in flexible electronics applications. The plastic foil was attached onto a rigid handling wafer during deposition and structuring. A 4 nm Chromium layer was deposited before the Bi for better adhesion. It is noteworthy that sputter deposited Bismuth films in general exhibit a high surface roughness due to the development of microscopic hillocks during deposition (see AFM picture in Figure 2e). The roughness (Rq value) of the prepared 2 µm thick films in this study was determined by AFM to be around 300 nm over the displayed area of 20 x 20 μm^2. In Figure 2f a line profile from the AFM image is provided showing individual hillocks of up to more than 2 µm in height. However, a nanoscale mechanical polishing method is available in order to remove the hillocks without influencing the sensing capabilities of the Bi layer [22].

After deposition, the Bi films were structured into a Hall cross geometry by lithography. (Figure 2b and 2d) At first, photoresist (ARP 3510, Allresist GmbH) was spin-coated onto the Bi layer with 3500 revolutions per minute for 35 seconds and baked in an oven at 80 °C for 30 minutes under Nitrogen flow. Then, Exposure with 365 nm UV light at 275 W was performed through a Cr mask using a mask aligner (MA 56, Suss Micro Tec) for 8 seconds, followed by a resist development (ARN 300-35, Allresist GmbH; diluted with H_2O 1:1). The Hall cross geometry was then defined by ion beam etching (IBE) in an Ar atmosphere at 600 eV (MicroSys 500; Roth & Rau AG). If not stated differently the active area of the structured Hall crosses is 1 x 1 mm^2 as shown in Figure 2d.

After removal of the residual photoresist by rinsing in acetone and isopropanol and subsequent drying in nitrogen gas flow, the flexible PEEK membrane with the patterned Hall cross was released from the handling wafer. Individual Hall elements were cut from the prepared array of Bi crosses.

3.3 Contacting and Packaging of Sensors

Thin Bismuth films are known to be mechanically damageable, which demands a sufficient protective encapsulation during the experimental investigations. In this work, we used adhesive tape for protection. Before encapsulation, the tape was perforated in a squared arrangement (4 x 4 mm^2) with a 1 mm biopsy punch to determine the van der Pauw contact geometry. The four holes were aligned with the four contact ends of the patterned Hall cross as the Bismuth film was covered with the adhesive tape. This allows for an accurate and reliable contacting while the Bismuth cross remains protected between the PEEK substrate and the adhesive tape. Figure 2d shows a Bi cross buried underneath the transparent adhesive tape before contacting. One of the perforations is also visible on the right side of the image with the exposed Bismuth surface for contacting. For equal thicknesses and comparable mechanical parameters of the substrate and cover material, a thin Hall element can be operated in the neutral mechanical plane [20] of a flexible plastic sheet. This minimizes mechanical stresses on the functional parts and allows for an improved flexibility of the final device as smaller bending radii can be achieved.

The electrical contacts were realized with thin (62 µm) isolated copper wires and conductive silver paste through the perforated holes in the cover tape. In order to reduce disturbances from Eddy currents during operation of the prepared sensors in the levitating ball setup, loops in the conducting parts have to be avoided. Therefore, the

wires were twisted until above the Hall cross and then led to the four contact points along the four branches (Figure 2b). The electrical resistance along two opposing contacts of the prepared Hall sensors (1 mm branch width) is around 15 Ω. Finally, another adhesive tape was attached on top of the wired sensor to stabilize the contacts and fix the twisted wire. A conceptual cross section of the final Hall probe including one contact site is shown in Figure 2c. A photograph of the final Bi sensor device attached to a curved surface of a sample holder (bending radius: 22 mm) is provided in Figure 2a. The prepared sensors have a maximum thickness of 280 µm including the contact wires, however the largest contribution (about 150 µm) is due to the twisted cables. The encapsulated sensor cross before contacting, as shown in Figure 2d, has a total thickness of only 80 µm.

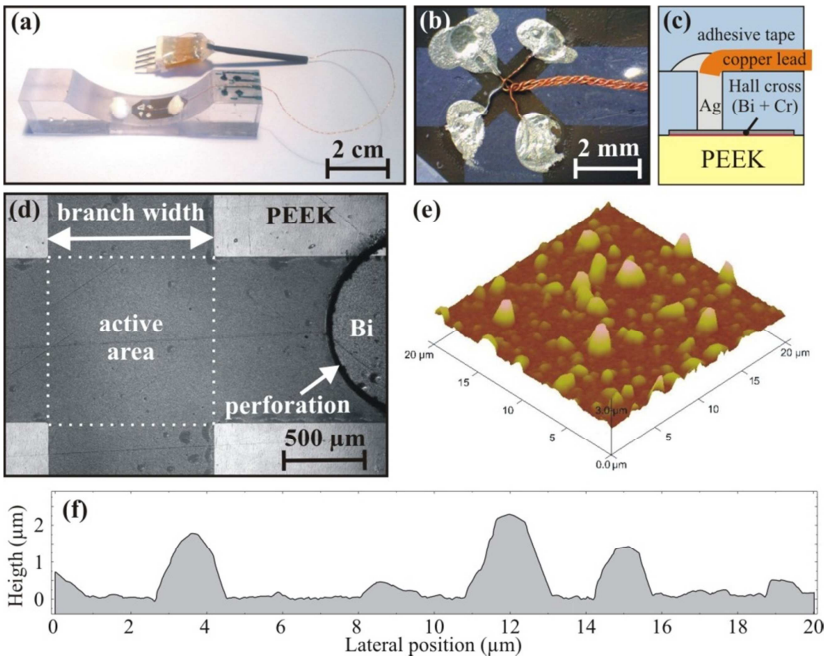

Figure 2: Ultra-thin and flexible Hall sensor device (a) Photograph of the final device mounted to the curved surface of a sample holder. (b) Microscopic close-up of the sensor with contact wires above the encapsulated Bismuth cross. (c) Conceptual cross section of the sensor device showing one contact site. (d) Optical micrograph of the active sensor area (1 x 1 mm²) underneath the capping before contacting. The branch width of 1 mm is indicated. On the right side of the image one of the contact perforations with the exposed Bismuth film is visible. (e) AFM image of the sputter deposited 2 µm thick Bi surface (20 x 20 µm^2). (f) AFM line profile showing several hillocks.

3.4 Characteristics

The fabricated Bismuth probes where characterized in a Hall measurement setup in dependence of different parameters (i.e. size, temperature and bending radius). A constant current of 50 mA was passed along two opposing branches of the structured cross and the voltage was recorded along the remaining two contacts while the out-of-plane magnetic field was swept with an electromagnet. The experimentally obtained data was offset corrected and fitted linearly to obtain the Hall sensitivity for direct comparison.

3.4.1 Size Dependence

In order to determine the optimal size of the Bi Hall crosses, specimens of different branch widths were structured and measured at room temperature. The branch width d defines the active area A of the Hall cross by $A = b^2$ (Figure 2d). Figure 3 summarizes the experimental results for sizes between 0.5 x 0.5 mm^2 and 3 x 3 mm^2. Smaller Bi structures tend to delaminate from the PEEK substrate during the etching process.

The data shows the linear Hall signal for magnetic fields in the range of ±2 T. The linear fits of each measurement are given in solid lines. The inset summarized the Hall sensitivities in dependence of the branch width of the respective Bi cross structure. The sensitivity of the prepared sensors reaches a maximum for 1 x 1 mm^2 size. According to Hall effect theory the generated Hall voltage is proportional to the perpendicular current density. For larger branch widths and a constant supply current the current density decreases, and thus the Hall sensitivity is reduced. The decrease for a sensor size below 1 x 1 mm^2 is attributed to the heating of the Bismuth layer by the supply current. Hence, Hall crosses with a branch width of 1 mm are used throughout the following investigations.

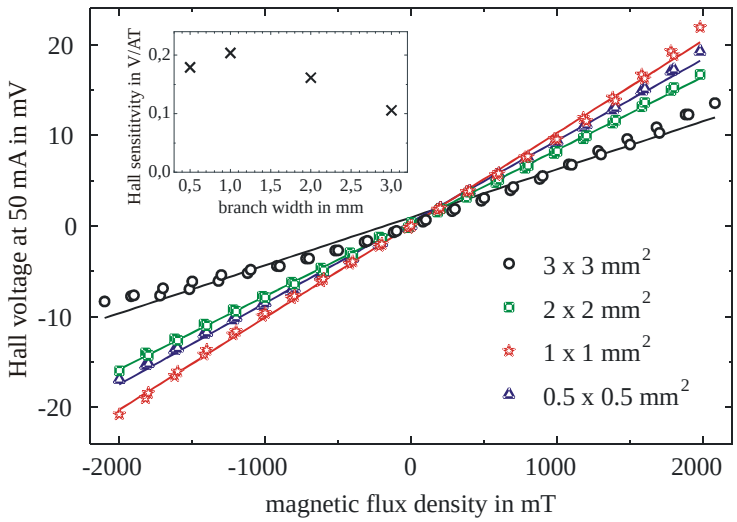

Figure 3: Hall characteristic for different Bi cross sizes at 50 mA supply current. The inset shows the Hall sensitivity in dependence of the branch width.

3.4.2 Temperature Dependence

The Hall effect in general is temperature dependent, mainly due to a reduction of charge carrier mobility with heat in a conductor. However, the usage of Hall probes in narrow air gaps of magnetic bearings requires a reliable flux measurement at operation temperatures between 60–80 °C, as well as during a warm up from ambient temperatures. In order to quantify the temperature dependence, an as prepared Hall sensor was mounted on a Peltier element (ETH-127-14-15, Global Component Sourcing) equipped with an active heat exchanger inside the Hall characterization setup. The Peltier element generated temperatures of -20 to 80 °C on the Hall sensor controlled by a surface contact thermocouple. The recorded Hall data in this temperature range is plotted in Figure 4.

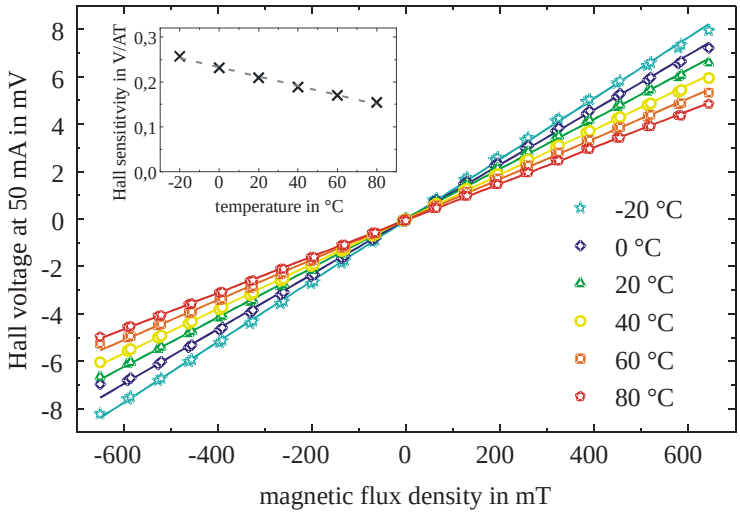

Figure 4: Hall characteristics for different temperatures at 50 mA supply current. The inset shows the Hall sensitivity in dependence of the temperature and a linear fit of the experimental data.

Due to the height occupied by the Peltier element and the heat exchanger between the pole shoes of the Hall test setup (about 30 mm) the magnetic field could be swept only between ±650 mT during this investigation. However, as demonstrated already in the previous subchapter, the slope is not expected to vary for higher fields. As expected, the slope of the Hall characteristic decreases with increasing temperature. As shown in the inset, the Hall sensitivity decreases in a linear fashion. The slope of the linear fit shown in the inset gives a value of about -1 mV/ATK. The temperatures in this investigation represent a realistic operation range for magnetic bearings. Hence, the flexible magnetic field sensors presented here would require an additional temperature compensation for magnetic bearings applications.

3.4.3 Flexibility Test

In flux controlled AMBs the magnetic field sensor should be placed onto the concave surface of the stator pole shoes for a quantitative and reliable flux measurement. Thus, different sizes of magnetic bearings require the sensors to operate at different bending radii. The performance of the presented Bi Hall sensors upon bending is subject of this investigation. A prepared sensor was successively mounted and characterized on three sample holders with different concave curvatures simulating typical sizes of magnetic bearings. The results are plotted in Figure 5.

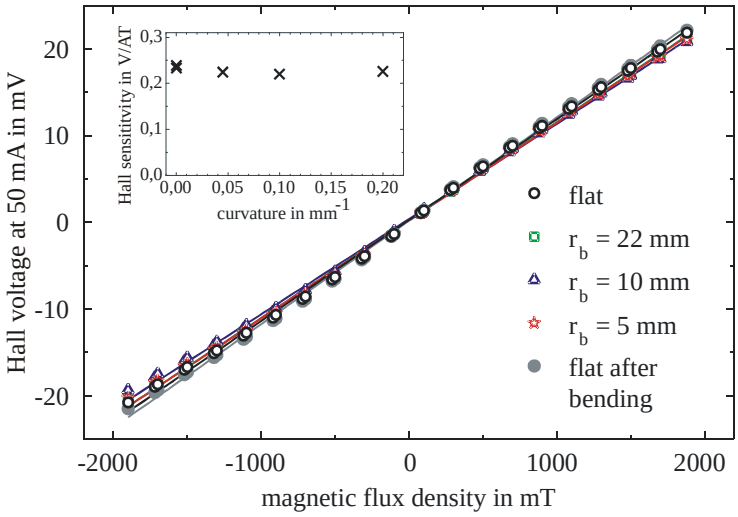

Figure 5: Hall characteristic for different sensor bending radii of the sensor at 50 mA supply current. The inset shows the Hall sensitivity in dependence of the sensor curvature.

Due to the height of the sample holders (8 mm) between the pole shoes of the Hall test setup, the magnetic field could be swept only between ±1.9 T during this investigation. For different bending radii of the prepared flexible sensor the data shows only very small variations of the Hall sensitivity (inset in Figure 5). These deviations are ascribed to small random misalignments during the fixture of the sensor to the different sample holders. This investigation clearly shows the functionality of the prepared Hall sensor with different bending radii, which qualifies them for the usage in magnetic bearings and on curved surfaces of other electrical machines.

3.4.4 Signal Processing and Signal-to-Noise Ratio

Due to the sensitivity of ≈200 mV/AT (at a temperature of 40 °C) the Hall voltage needs to be conditioned by a two level amplification and offset compensation during experimental studies in the levitating ball setup. For this purpose, we use low noise instrumentation amplifiers with a total amplification factor of $G = 15000$ to achieve a signal sensitivity of 30 V/T ($i_{Hall} = 10$ mA powered by a high precision power supply, $B_{max} = 200$ mT). Using a 12 bit analog-digital-converter (ADC), we achieve a theoretical resolution of 48.8 µT. The amplified signal of the Bi Hall sensor shows basic noise and irregular disturbances, which might be caused by capacitive effects or eddy currents inside the sensor element. It was found, that disturbances decrease nonlinear with the reduction of supply current. As at $i_{Hall} = 10$ mA the sensor showed the smallest disturbances, this value was chosen for the performed experiments. Similar to the commercial reference sensor, the noise (peek-peek) of the flexible Hall sensor amounts to $u_{P\text{-}P} \approx 30$ mV ($\Delta f = 200$ MHz) after amplification. The observed irregular disturbances increase the total noise to $u_{P\text{-}P} \approx 150$ mV. The signal-to-noise ratio is decreased from 67.5 dB to 47.4 dB. Thereby, with the flexible Bi Hall sensor a resolution of 0.88 mT including ADC quantization noise was achieved.

3.4.5 Sensor Parameters

The results of the performed characterizations and key parameters of the fabricated flexible Hall probes are summarized in Table 2.

Parameter		Value	Unit
Sensor dimensions	Total cross size (distance of contact points)	4	mm
	Active area	1x1	mm²
	Bismuth film thickness	≈2	µm
	Total height (before contacting)	80	µm
	Total height (after contacting)	≈280	µm
Electrical parameters	Supply current (for characterizations)	50	mA
	Supply current (for experiments)	10	mA
	Supply side internal resistance	≈15	Ω
	Hall side internal resistance	≈15	Ω
	Hall sensitivity (before amplification)	≈200	mV/AT
	Sensor resolution	0.88	mT
	Signal-to-noise ratio $SNR_{noise\ and\ disturbance}$	47.4	dB
	Signal-to-noise ratio $SNR_{noise\ only}$	67.5	dB
Other parameters	Operating temperature range (tested)	-20 to 80	°C
	Temperature coefficient of sensitivity	≈1	mV/ATK
	Maximum operating curvature (tested)	0.2	mm^{-1}

Table 2: Sensor parameters.

4 Control Strategies

4.1 Magnetic Bearing Plant

Prior to the control structure design, the magnetic bearing plant has to be identified and derived by means of state space description. Figure 6 shows the complete scheme of the AMB setup including the electromagnetic and mechanical plant. The system is driven by the power electronics (H-bridge) simplified as a dead time element. The coil can be modeled as a PT1 element. The system exhibits positive feedback since the magnetic resistance R_m depends on the position x.

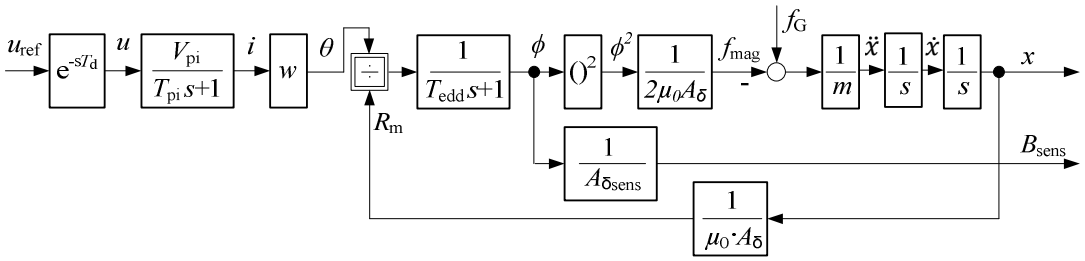

Figure 6: Scheme of a magnetic bearing with electromagnetic and mechanical plant.

The specific AMB setup is characterized by an inhomogeneous magnetic field, which depends in strength and profile on the coil current i and ball position x. Thus, the effective working pole surface A_δ varies with the ball's position. For different magnetic fields the ratio of magnetic working area A_δ and local measurement area $A_{\delta sens}$ as well as the ratio of flux and stray flux are not constant. Thus, the magnetic flux density B_{sens} measured by the flexible sensor depends on the coil current as well as the position. Based on the experimental data of the plant identification the characteristic diagram of $B(x,i)$ is approximated and described by Equation (1).

$$B(x,i) = \frac{i}{ax^2 + bx + c} \tag{1}$$

Furthermore the coil voltage characterized by the coil current and derivatives of position and current is given in Equation (2).

$$u = L \cdot \frac{\mathrm{d}i}{\mathrm{d}t} + k_\mathrm{u} \cdot \frac{\mathrm{d}x}{\mathrm{d}t} + R \cdot i \tag{2}$$

Since the inner flux density loop is very fast in comparison to the mechanical plant it can be presumed that the term dx/dt is zero. Based on this assumption and Equation (1) the derivative of the magnetic flux density is derived in Equation (3).

$$\dot{B} = -\frac{R}{L} \cdot B - \frac{2ax + b}{ax^2 + bx + c} \cdot B\dot{x} + \frac{1}{L} \cdot \frac{1}{ax^2 + bx + c} \cdot u \tag{3}$$

Now the magnetic force f_{mag} for the experimental setup has to be analyzed. It can be described in dependence of coil current and position as well as of flux density and position. Based on force measurements the nonlinear characteristic of the magnetic force as a function of coil current and position is described in Equation (4).

$$f_{mag}(x, i) = q_1 e^{q_2 x} i^{q_3} \tag{4}$$

The coil current is replaced by Equation (1) to obtain the magnetic force as a function of magnetic flux density and position in Equation (5). All coefficients of Equation (1) and (4) were calculated by an approximation of the measured data and are specified in Table 3.

$$f_{mag}(x, B) = q_1 e^{q_2 x}((ax^2 + bx + c)B)^{q_3} \tag{5}$$

In accordance to Figure 6 the modeling of the mechanical plant is based on Equation (6). From Equation (5) the second derivative of the ball´s position $\ddot{x}$ is obtained. By means of Equation (3) and (7) the state vector is given in Equation (8).

$$f_{mag} + m\ddot{x} = 0 \tag{6}$$

$$\ddot{x} = -\frac{1}{m} q_1 e^{q_2 x}\left((ax^2 + bx + c)B\right)^{q_3} \tag{7}$$

$$\mathbf{x} = \begin{bmatrix} x \\ \dot{x} \\ B \end{bmatrix} = \begin{bmatrix} x_1 \\ x_2 \\ x_3 \end{bmatrix};\ \dot{\mathbf{x}} = \begin{bmatrix} x_2 \\ -\frac{1}{m} q_1 e^{q_2 x_1}\left((a{x_1}^2 + bx_1 + c)x_3\right)^{q_3} \\ -\frac{R}{L} x_3 - \frac{2ax_1 + b}{a{x_1}^2 + bx_1 + c} \cdot x_2 x_3 + \frac{1}{L} \frac{1}{a{x_1}^2 + bx_1 + c} \cdot u \end{bmatrix} \tag{8}$$

Coefficient $B(x,i)$	Value	Coefficient $f_{\mathrm{mag}}(x,i)$	Value
a	-73526 A/Tm^2	q_1	0.16 N/A
b	1581 A/Tm	q_2	-186 1/m
c	24 A/T	q_3	1.44

Table 3: Experimentally determined plant coefficients.

4.2 Linear control

After the parameter identification and system description of the one-axis AMB plant, we continue with a quasi-continuous controller design to test the flexible sensor elements and to compare the flux based algorithm with a

current based one. As a first step, a linear algorithm is considered. Therefore, we have chosen a cascaded structure consisting of closed loop position control with a subordinated flux density loop. (Figure 7)

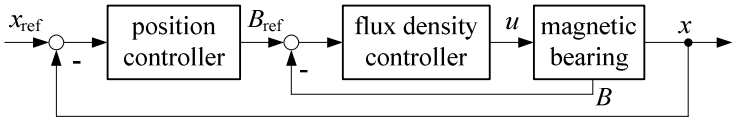

Figure 7: Scheme of cascaded position control with subordinated flux density loop.

For the flux density controller design the transfer function of the flux density plant is required. For this purpose, we can reduce $\dot{x_3}$ given in Equation (8). Presuming a chosen operating point (x_0) it is assumed that the position is constant and the ball´s velocity $\dot{x}$ is zero. After applying the Laplace transformation on the simplified function $\dot{x_3}$ the transfer function of the flux density plant is obtained in Equation (9). Additional time constants caused by pulse width modulation and eddy current effects are summarized in T_σ. Thus, the transfer function (Equation (10)) is amended by an additional PT1 element representing T_σ.

$$G_{\mathrm{plantB}}(s) = \frac{B(s)}{U(s)} = \frac{K_{\mathrm{plantB}}}{T_{\mathrm{plantB}}s + 1}\ ;\ K_{\mathrm{plantB}} = \frac{1}{R(ax_0^2 + bx_0 + c)}, T_{\mathrm{plantB}} = \frac{L}{R} \tag{9}$$

$$G_B(s) = \frac{B(s)}{U(s)} = \frac{K_{\mathrm{plantB}}}{\left(T_{\mathrm{plantB}}s + 1\right)(T_\sigma s + 1)} \tag{10}$$

To control the given plant a proportional integral (PI)-structure is used. It is parameterized to achieve good reference response on the control system. The plants response time can be compensated by the reset time (Equation (11)).

$$G_{\mathrm{PI\_B}}(s) = K_{\mathrm{P\_B}}\left(1 + \frac{1}{T_{\mathrm{N\_B}}s}\right) \text{with } T_{\mathrm{N\_B}} = T_{\mathrm{plantB}}, K_{\mathrm{P\_B}} = \frac{T_{\mathrm{N\_B}}}{2K_{\mathrm{plantB}}T_\sigma} \tag{11}$$

At this stage a controller has to be chosen to stabilize the naturally instable position plant. After linearization of Equation (7) and Laplace transformation we obtain the transfer function of the position plant $G_{\mathrm{plantx}}(s)$, characterizing the dynamic behavior by force-position factor k_{x} and force-flux density factor k_{B} (Equation (12)). To stabilize the instable second order plant, a conventional proportional-integral-derivative (PID) controller is used. The stiffness k and damping ratio D are adjusted by parameters given in Equation (13).

$$G_{\mathrm{plantx}}(s) = \frac{X(s)}{B(s)} = \frac{\frac{k_{\mathrm{B}}}{m}}{s^2 - \frac{k_{\mathrm{x}}}{m}};\ k_{\mathrm{x}} = m\ddot{x}_0\left(-q_2 - \frac{(2ax_0 + b)q_3}{ax_0{}^2 + bx_0 + c}\right), k_{\mathrm{B}} = \frac{-m\ddot{x}_0 q_3}{B_0} \tag{12}$$

$$G_{\mathrm{PIDx}}(s) = K_{\mathrm{P\_x}}\left(1 + T_{\mathrm{V\_x}}s + \frac{1}{T_{\mathrm{N\_x}}s}\right) \text{ with } K_{\mathrm{P\_x}} = \frac{k + k_{\mathrm{x}}}{k_{\mathrm{B}}} \text{ and } T_{\mathrm{V\_x}} = \frac{2D\sqrt{km}}{K_{\mathrm{P\_x}}k_B} \tag{13}$$

4.3 Nonlinear control

To improve performance of the AMB, flatness based feed forward control with optional trajectory generation was designed. The method is well-known to control nonlinear flat systems. Detailed descriptions on theoretical fundamentals as well as system conditions concerning flatness are presented elsewhere [23,24]. Figure 8 shows the basic concept of this control strategy. Each controller consists of a stabilizing component and a linearizing algorithm to compensate the original nonlinear dynamics of the plant [23].

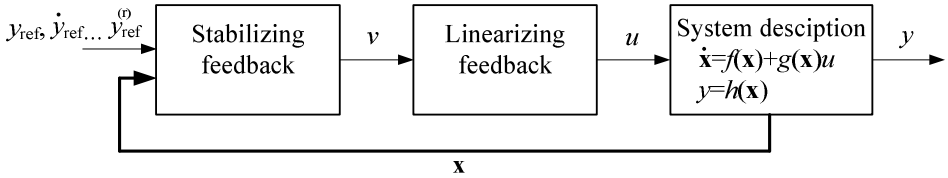

Figure 8: Scheme of flatness based feed forward control.

In accordance to Figure 8, the state space description for the each subsystem has to be derived. The Lie derivatives as well as the relative degree *r* of the system have to be determined and the controller output *u* is calculated via Equation (14). The virtual system input *v* of the linearizing feedback component is provided by the stabilizing algorithm. For this purpose, a linear controller is used corresponding to Equation (15). In order to avoid steady-state deviations, an integral component with anti-windup can be added to the stabilizing controller.

$$u = \frac{1}{L_G \cdot L_f^{r-1} \cdot h(\mathbf{x})} \left(-L_f^r \cdot h(x) + v\right) \tag{14}$$

$$v = y_{\text{ref}}^{(r)} - \sum_{i=0}^{r-1} k_i \left(e^{(i)}\right) \text{ with } e^{(i)} = (y^{(i)} - y_{\text{ref}}^{(i)}) \tag{15}$$

Figure 9 illustrates the detailed structure that is used for the test setup. For both, the flux density as well as the position plant a separate controller is used. Since only position and flux density were measured, the balls velocity $\dot{x}$ is obtained by the differential quotient $\Delta x/\Delta t$. It is noteworthy, that a velocity observer may further improve the AMB´s performance.

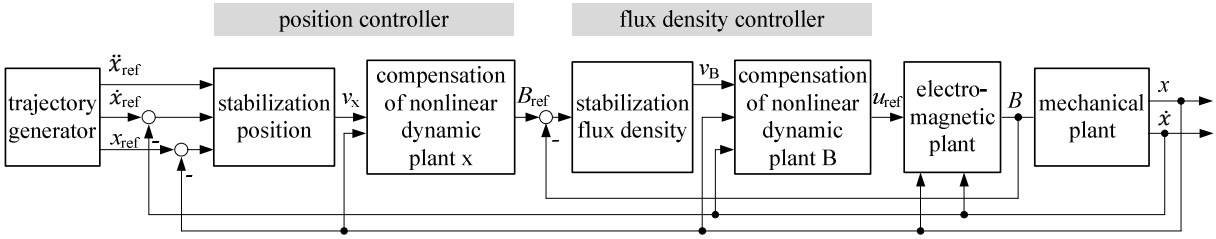

Figure 9: Scheme of flatness based feed forward control.

Flux density controller design is based on Equations (8), (16) and (17). Here, flux density $B=x_3$ is the system output.

$$\dot{x}_3 = \left(-\frac{R}{L} \cdot x_3 - \frac{2ax_1 + b}{a{x_1}^2 + bx_1 + c} \cdot x_2 x_3\right) + \left(\frac{1}{L} \frac{1}{a{x_1}^2 + bx_1 + c}\right) \cdot u \tag{16}$$

$$\dot{x}_3 = f(\mathbf{x}) + g(\mathbf{x}) \cdot u;\ y = x_3 = h(\mathbf{x}) \tag{17}$$

By means of Lie derivatives, a relative degree of $r = 1$ is determined. Due to the higher sample rate of flux density measurement, we conclude that position as well as velocity can be assumed as momentary constants. Hence, the systems possesses an order of $n = 1$ and is therefore defined as flat. Given that, the controller output u_{ref} can be calculated via Equation (18).

$$u_{\text{ref}} = L(ax^2 + bx + c)\left(\frac{2ax + b}{ax^2 + bx + c}\right)\dot{x}B - \frac{R}{L}B + v_{\text{B}} \tag{18}$$

The stabilization of the system occurs in accordance to Equation (19). For the test setup a common PI controller is used.

The derivative $\dot{x}_{3\mathrm{ref}}$ is set to zero, because the flux density controller has to follow its reference variable B_{ref} rather than a generated trajectory.

$$v_{\mathrm{B}} = \dot{x}_{3\mathrm{ref}} - k_{0\_\mathrm{B}} e_{\mathrm{B}} - k_{\mathrm{I\_B}} \int (e_{\mathrm{B}}(\tau)) d\tau \tag{19}$$

The position controller is designed similar to the flux density controller. Equation (8) provides the system description of the mechanical AMB plant. Furthermore gravity was added to model the overall system with external influence, summarized in Equation (20) and (21).

$$\dot{\mathbf{x}} = \begin{bmatrix} x_2 \\ g \end{bmatrix} + \begin{bmatrix} 0 \\ -\frac{m}{q_1 e^{q_2 x} (ax^2 + bx + c)^{q_3}} \end{bmatrix} \tilde{x}_3 \text{ with } \tilde{x}_3 = x_3^{q_3} \tag{20}$$

$$\dot{x}_3 = f(\mathbf{x}) + g(\mathbf{x}) \cdot \tilde{x}_3;\ y = x_1 = h(\mathbf{x}) \tag{21}$$

This system is characterized by a relative degree of $r = 2$ and the plant is of second order as well. Hence, the controller output B_{ref} of the flat system can be calculated with respect to Equation (22).

$$B_{\mathrm{ref}} = \left(\frac{m}{q_1 e^{q_2 x} (ax^2 + bx + c)^{q_3}} (g - v_{\mathrm{x}}) \right)^{q_3} \tag{22}$$

In accordance to Equation (15) the mechanical system is stabilized by a PID control algorithm (Equation (23)). The reference variables are calculated by a trajectory generator considering the dynamic limitations of the system as well as the limited operating range $0 \leq x \leq 12$ mm. Since the system is not able to realize negative forces the balls acceleration is limited by gravity ($\ddot{x}_{1\mathrm{ref}} \leq g$).

$$v_{\mathrm{x}} = \ddot{x}_{1\mathrm{ref}} - k_{0\_\mathrm{x}} e_{\mathrm{x}} - k_{1\_\mathrm{x}} \dot{e}_{\mathrm{x}} - k_{\mathrm{I\_x}} \int (e_{\mathrm{B}}(\tau)) d\tau \text{ with } k_{0\_\mathrm{x}} = \frac{k}{m}, k_{1\_\mathrm{x}} = 2D\sqrt{\frac{k}{m}} \tag{23}$$

5 Experimental Results

5.1 Cascaded Linear Control Algorithm

5.1.1 Stabilization at Constant Position

Using the flexible Bismuth Hall sensors we tested the complete setup with different control structures as described in Chapter 4. At first the positioning performance for constant reference position as well as step and disturbance response was analyzed. The operating point was chosen to be at $x_0 = 10$ mm. Linear cascaded control algorithms were used and an inner closed flux loop control by use of Bismuth and commercial Hall probe was compared to a closed current loop control. For a constant reference the positioning accuracy is shown in Figure 10.

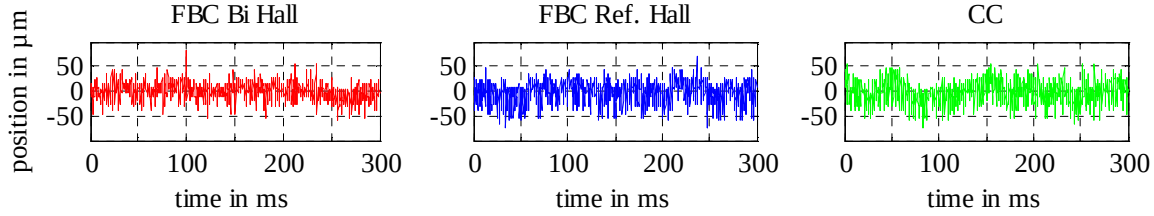

Figure 10: Positioning at operating point x_0, k = 100 N/m, D = 1.0 (FBC Flux based control, CC Current control).

On this basis the functionality and performance of the flexible Bismuth sensor operating in the AMB setup can be assessed. Flux based control with Bi Hall sensor achieves a positioning accuracy of $\Delta x \approx 40\,\mu m$, whereas with current control positioning is within the range of $\Delta x \approx 60\,\mu m$. Using the Bismuth based Hall sensor the accuracy even exceeds the value of the commercial reference sensor.

5.1.2 Response Characteristics

Step responses for upward as well as downward motion are presented in Figure 11. This data shows that flux control gains with reduced deviation of up to 30 % and smaller response times. Especially in the case of low damping ratios the current based control shows increased overshooting for a down-step reference signal.

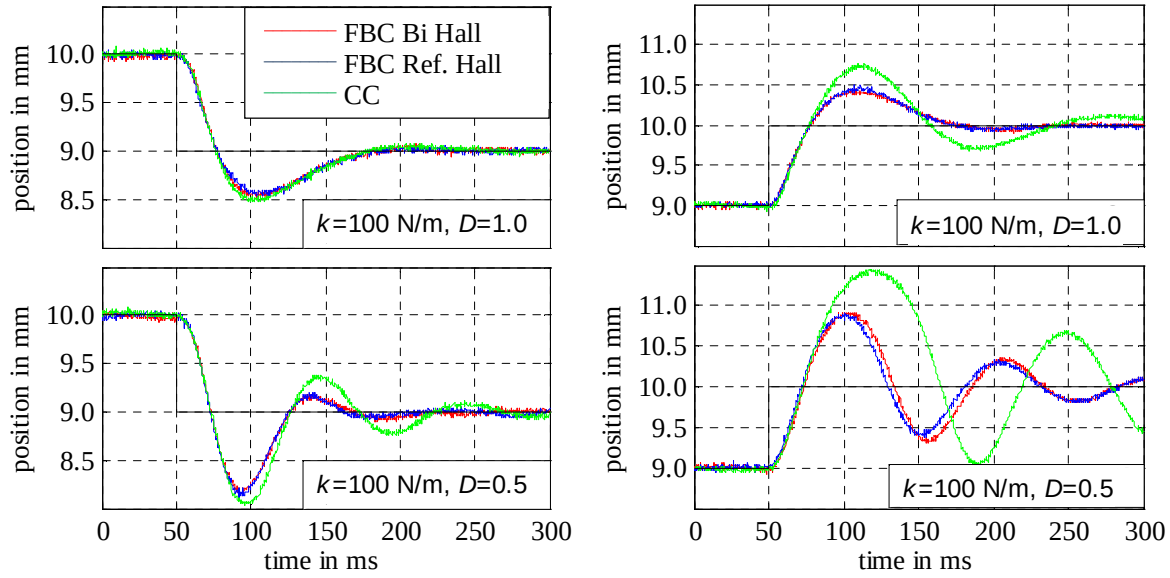

Figure 11: Response characteristics. Step Δx_{ref} = 1 mm, upward and downward.
(FBC Flux based control, CC Current control)

5.1.3 Disturbance Characteristics

In order to test disturbance characteristics the load dropping method was chosen to simulate a sudden disturbing force. An additional mass of m_{drop} = 10 g was mounted at the ball as shown in Figure 12. Due to the lack of pre-triggering, the disturbance response was recorded as the twine was cut (Figure 13). Again, the flux based control gains with reduced overshooting. The response time of current control is smaller, though the decay rate is marginally higher.

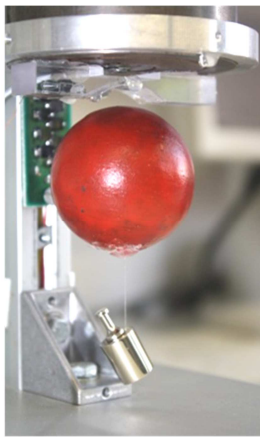

Figure 12: Load drop setup.

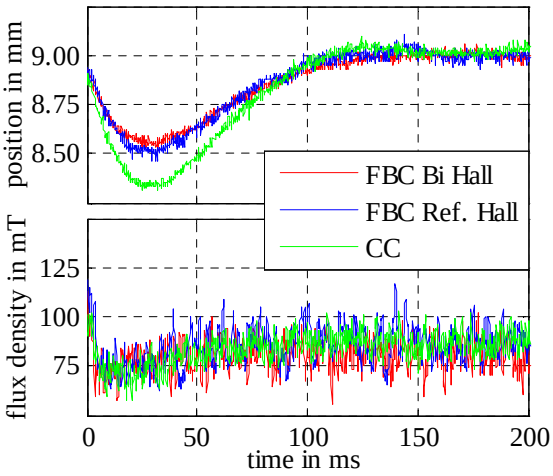

Figure 13: Disturbance response after load drop.
(FBC Flux based control, CC Current control)

5.2 Flatness Based Feed Forward Control with Trajectory Generation

After comparing linear flux and current based controls, experimental data for a flatness based control algorithm is presented. Figure 14 shows the positioning accuracy for the operating point at $x_0 = 10$ mm. Compared to linear controls the accuracy is improved by a factor of 2 and deviations smaller than $\Delta x = 20$ µm were achieved together with smoother flux densities and coil currents (data not shown).

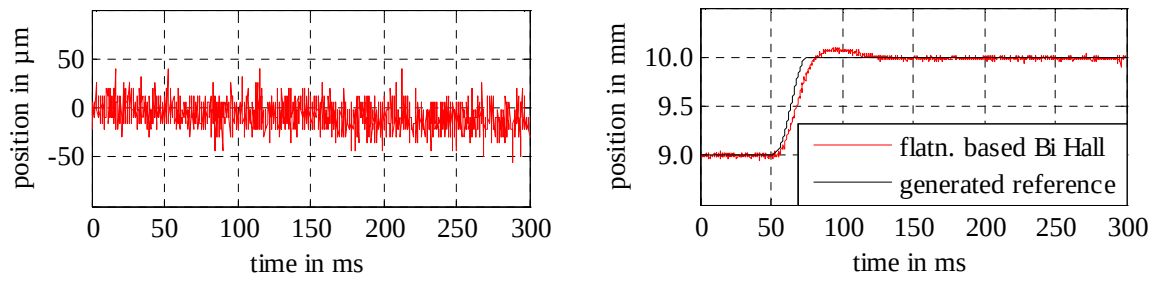

Figure 14: Position accuracy and downward motion using flatness based control with generated trajectory.

For this approach the generation of trajectories to realize up- and downward motions is discussed. In accordance to the dynamic limits of the system a trajectory is calculated to perform the position step of $\Delta x = 1$ mm. Figure 14 also shows the positioning of the levitating ball for a downward movement. Due to coefficient uncertainties, varying setup parameters and aerodynamic drag the position does not exactly follow its reference. However, the proposed flatness based control shows superior effectiveness regarding controller design and gains with extreme low overshooting of about 100 µm.

6 Conclusion

For the first time, ultra-thin and flexible Bi Hall sensors were fabricated and characterized. On a proof-of-concept level the integration into a flux density controlling loop of AMBs was demonstrated. The experimental investigations have shown that flux based control gains with higher performance compared to current based control.

Linear and nonlinear control strategies with flux density feedback as well as specific characteristics of the Hall sensor were presented in this work. Experimental results on dynamic performance of AMBs using flexible sensors were discussed together with the signal-to-noise ratio, response to disturbances as well as thermal and mechanical sensor characteristics.

Compared to current based control, the linear flux density control using the flexible Bismuth Hall sensor showed reduced overshooting (up to 30 %) and smaller response times after reference steps. After load disturbances the displacement was reduced to 75 %, whereas the achieved response time was similar to current based control. For the operation with a commercial reference Hall sensor made of gallium arsenide a similar behavior was detected for this experimental setup. Moreover, the performance can be improved with a flatness based control using flux density feedback and trajectory generation. Therewith the overshooting is reduced to 25 % in comparison to linear control.

Despite the proof-of-concept presented in this study, the reported ultra-thin and flexible Bismuth based Hall sensors are at an early stage of development. Sensor components in AMBs are expected to exhibit a design life of more than 10 years, however, no long term stability tests were performed at this time. Furthermore, the total sensor thickness that is required for usage in real AMBs is about 150 µm. At this stage the proposed flexible Hall sensor has a thickness of about 280 µm. The encapsulation and contacting with rigid copper wires and conductive silver paste make up the largest part of the sensor height (250 µm) and therefore need to be improved. For further reduction of the overall device thickness deposited thin film contact leads on top of the encapsulating layer and through the perforations are conceivable. In addition, even thinner substrate and encapsulation foils might be used.

For more sensitive Hall probes the film thickness and size of the Bismuth cross can be reduced, and other deposition methods could lead to higher film quality and texture as well as to a reduction of fabrication costs. However, the experimental results presented in this work are promising for the realization of suitable flux gauges and their application in commercial AMBs to enhance stiffness and allow for precise rotor positioning.

References

[1] Xiaofei. Chen, K. Lie and K. Xiao . A Novel Force Feedback Controller for Active Magnetic Bearings. In *Proceedings of the 11th International Symposium on Magnetic Bearings (ISMB)*, Nara, 2008.

[2] J. H. Yi, K. H. Park, S. H. Kim, Y. K. Kwaik, M. Abdelfatha, and I. Busch-Vishniac. Force Control for Magnetic Levitation System Using Flux Density Measurement. In: *34th Conference on Decision and Control*. New Orleans, 1995.

[3] Hannes Bleuler, D. Vischer, G. Schweitzer, A. Traxler, and D. Zlatnik. New Concepts for cost-effective Magnetic Bearing Control. *Automatica*, Vol. 30, No. 5, S. 871-876, New Orleans, 1995.

[4] Panagiotis Tsiotras. Low-Bias Control of AMB Subject to Voltage Saturation: State-Feedback and Observer Designs. *IEEE Trans. Control Syst. Technol.,13(2), 2005.*

[5] Dae-Hyeong Kim, J. Xiao, J. Song, Y. Huang, and J. A. Rogers. Stretchable, Curvilinear Electronics Based on Inorganic Materials. *Adv. Mater.*, 22(19), 2010.

[6] Tsuyoshi Sekitaki and T. Someya. Stretchable, Large-area Organic Electronics. *Adv. Mater.*, 22(19), 2010.

[7] Stuart S. P. Parkin. Flexible giant magnetoresistance sensors. *Appl. Phys. Lett.*, 69(20), 1996.

[8] Yuan-fu Chen, Y. Mei, R. Kaltofen, J. I. Mönch, J. Schumann, J. Freudenberger, H.-J. Klauß, and O. G. Schmidt. Towards flexible magnetoelectronics: Buffer-enhanced and mechanically tunable GMR of Co/Cu multilayers on plastic substrates. *Adv. Mater.*, 20(17), 2008.

[9] Clement Barraud, C. Deranlot, P. Seneor, R. Mattana, B. Dlubak, S. Fusil, K. Bouzehouane, D. Deneuve, F. Petroff, and A. Fert. Magnetoresistance in magnetic tunnel junctions grown on flexible organic substrates. *Appl. Phys. Lett.*, 96(7), 2010.

[10] Michael Melzer, D. Makarov, A. Calvimontes, D. Karnaushenko, S. Baunack, R. Kaltofen, Y. Mei, and O. G. Schmidt. Stretchable Magnetoelectronics. *Nano Lett.*, 11(6), 2011.

[11] Michael Melzer, D. Karnaushenko, D. Makarov, L. Baraban, A. Calvimontes, J. I. Mönch, R. Kaltofen, Y. Mei and O. G. Schmidt. Elastic magnetic sensor with isotropic sensitivity for in-flow detection of magnetic objects. *RSC Adv.*, 2(6), 2012.

[12] Horacio V. Estrada and IEEE. A MEMS-SOI 3D-MAGNETIC FIELD SENSOR. In *24th IEEE International Conference on MEMS*, January 2011.

[13] Carl R. Knospe. Active magnetic bearings for machining applications. *Control Engineering Practice*, Vol. 15, Issue 3, pp. 307-313 March 2007.

[14] Conrad Gähler. *Rotor Dynamic Testing and Control with Active Magnetic Bearings.* PhD thesis. ETH No. 12718. 1998. ETH Zürich.

[15] Mohamed M. Abdelfatah and F. P. Emad. A comparison between Current and Flux Control in Magnetic Bearing Systems. *Proceedings of the American Control Conference*, San Francisco, 1993.

[16] Daniel Zlatnik and Alfons Traxler . Cost-Effective Implementation of Active Magnetic Bearings. In: *Proceedings of the 2nd International Symposium on Magnetic Bearings (ISMB)*, Tokyo, 1990.

[17] Thomas Schuhmann, W. Hofmann and R. Werner. Adaptive Linear and Extended Kalman Filter applied to AMB with Collocated Position Measuring. *Proceeding of the 10th International Symposium on Magnetic Bearings (ISMB)*, Martigny, 2006, pp. 6.

[18] Joe Imlach and R. W. Kipp. Development of an Integrated Flux / Position Sensor. In: *Proceedings of the 6th International Symposium on Magnetic Bearings (ISMB)*, Cambridge (Massachusets), 1998.

[19] Radinka Koseva, J. I. Mönch, J. Schumann, K.-F. Arndt, and O.G. Schmidt. Bismuth Hall probes: Preparation, properties and application. *Thin Solid Films*, 518(17), 2010.

[20] Sang-Il Park, J.-H. Ahn, X. Feng, S. Wang, Y. Huang, and J. A. Rogers. Theoretical and Experimental Studies of Bending of Inorganic Electronic Materials on Plastic Substrates. *Adv. Funct. Mater.*, 18(18), 2008.

[21] Adarsh Sandhu, H. Masuda, K. Kurosawa, A. Oral and S.J. Bending. Bismuth nano-Hall probes fabricated by focused ion beam milling for direct magnetic imaging by room temperature scanning Hall probe microscopy. *Electr. Lett.*, 37(22), 2001.

[22] Radinka Koseva, J. I. Mönch, D. Meier, J. Schumann, K.-F. Arndt, L. Schultz, B. Zhao and O. G. Schmidt. Evolution of hillocks in Bi thin films and their removal upon nanoscale mechanical polishing. *Thin Solid Films*, 520, 2012.

[23] Jean Lévine. *Analysis and Control of Nonlinear Systems. A Flatness-based Approach.* Springer, Berlin Heidelberg, 2009.

[24] Johannes von Löwis. *Flachheitsbasierte Trajektorienfolgeregelung elektromechanischer Systeme.* PhD thesis, Shaker, 2002.